Influence of Circumferential Flaw Length on Internal Burst Pressure of a Wall-Thinned Pipe

メタデータ	言語: English 出版者: 公開日: 2013-01-08 キーワード (Ja): キーワード (En): 作成者: TSUJI, Masataka, MESHII, Toshiyuki メールアドレス: 所属:
URL	http://hdl.handle.net/10098/7028

Manuscript Number: NED-D-12-00282R1

Title: Influence of Circumferential Flaw Length on Internal Burst Pressure of a Wall-Thinned Pipe

Article Type: Full Length Article

Corresponding Author: Mr. Masataka Tsuji,

Corresponding Author's Institution:

First Author: Masataka Tsuji

Order of Authors: Masataka Tsuji; Toshiyuki Meshii

Abstract: This paper examines the effect of the circumferential angle of a flaw on the internal burst pressure of pipes with artificial wall-thinned flaws.

The effect of the circumferential angle of a flaw has conventionally been regarded as unimportant in the evaluation of the internal burst pressure of wall-thinned straight pipes. Therefore, a burst pressure equation for an axial crack inside a cylinder, such as Kiefner's equation, has been widely applied. However, the following implicit assumptions notably exist when applying the equation to planar flaws in situations with non-planar flaws.

1） The fracture mode of the non-planar flaw under consideration is identical to that of the crack.

2） The effect of the circumferential angle of a flaw on the internal burst pressure, which is not considered for an axial crack, is small or negligible.

However, the experimental results from the systematic burst tests for carbon steel pipes with artificial wall-thinned flaws examined in this paper showed that these implicit assumptions may be incorrect. In addition, a simulation of this effect was conducted using a large strain elastic-plastic Finite Element Analysis (FEA) model.

The observed effects demonstrate that the burst pressure predicted for a crack with identical ligament thickness decreases with an increase in the circumferential angle of a flaw, so that the effect of the circumferential angle of a flaw on the internal burst pressure should be taken into consideration when evaluating internal burst pressure.

Influence of Circumferential Flaw Length on Internal Burst Pressure of a Wall-Thinned Pipe

Masataka TSUJI [a]*, Toshiyuki MESHII [b]

[a] Graduate Student, University of Fukui, 3-9-1 Bunkyo, Fukui, Fukui, JAPAN.

[b] Graduate School of Engineering, University of Fukui, 3-9-1 Bunkyo, Fukui, Fukui, JAPAN.

*Correspondent, E-mail: tsuji-m@u-fukui.ac.jp, FAX : +81-776-27-9764

Abstract

This paper examines the effect of the circumferential angle of a flaw θ on the internal burst pressure p_f of pipes with artificial wall-thinned flaws.

The effect of θ has conventionally been regarded as unimportant in the evaluation of the p_f of wall-thinned straight pipes. Therefore, a burst pressure equation for an axial crack inside a cylinder (Fig. 1, left), such as Kiefner's equation (Kiefner et al., 1973), has been widely applied (ANSI/ASME B31.G., 1991; Hasegawa et al., 2011). However, the following implicit assumptions notably exist when applying the equation to planar flaws in situations with non-planar flaws.

1) The fracture mode of the non-planar flaw under consideration is identical to that of the crack.

2) The effect of θ on p_f, which is not considered for an axial crack, is small or negligible.

However, the experimental results from the systematic burst tests for carbon steel pipes with artificial wall-thinned flaws examined in this paper showed that these implicit assumptions may be incorrect. In this paper the experimental results are evaluated in further detail. The purpose of the evaluation was to clarify the effect of θ on p_f. Specifically, the significance of the flaw configuration (axial length δ_z and wall-thinning ratio t_1/t) was studied for its effects on θ and p_f. In addition, a simulation of this effect was conducted using a large strain elastic-plastic Finite Element Analysis (FEA) model.

As observed from the experimental results, θ tended to affect p_f in cases with large δ_z, and t_1/t was also correlated with a decrease in p_f with an increase in θ. These tendencies were successfully simulated by the large strain elastic-plastic FEA model.

The observed effects demonstrate that the burst pressure predicted for a crack with identical ligament thickness decreases with an increase in θ, so that the effect of θ on p_f should be taken into consideration when evaluating p_f.

Key words: burst pressure, circumferential flaw length, wall-thinned pipes, Finite Element Analysis (FEA), fracture criterion, size effect

1. Introduction

A burst pressure equation for an axial crack inside a cylinder (Fig. 1, left), such as Kiefner's equation (Kiefner et al., 1973), is widely used (ANSI/ASME B31.G., 1991; Hasegawa et al., 2011) when evaluating the internal burst pressure of wall-thinned straight pipes. This engineering approach may be acceptable because the burst pressure of a crack (planar flaw) would likely yield a conservative estimate for flaws (non-planar flaw) in wall-thinned pipes. However, the following implicit assumptions exist when applying the equation for planar flaws to situations with non-planar flaws.

1） The fracture mode of the non-planar flaw under consideration is identical to that of the crack.

2） The effect on the burst pressure of the circumferential angle θ (shown in Fig. 1) of the non-planar flaw (which is not considered for an axial crack) is small or negligible.

With regards to fracture mode, the possibility of circumferential cracking cannot be overlooked because circumferential groove-like non-planar flaws have been observed in the circumferential weld line of a pipe due to Flow Accelerated Corrosion (FAC) (Duan et al., 2009).

The effect of the circumferential angle θ on the burst pressure p_f has been studied by Netto et al. (2005) and Oh et al. (2006). Using large strain elastic-plastic Finite Element Analysis (FEA), they showed that values of θ within a certain range (Netto: $0.03 \leq \theta/2\pi \leq 0.05$, Oh: $0.02 \leq \theta/2\pi \leq 0.08$;

groove-like flaws) do not affect p_f. Oh et al. verified their FEA results by experiments. However, the range of θ considered by this group was limited, so their examination regarding the effect of θ on p_f is not necessarily sufficient to cover all cases.

Based on the above-mentioned observations, this paper addresses the effect of θ on p_f specifically, and the purpose of this investigation is to clarify the effect of θ on p_f. For this purpose, systematic burst tests were conducted on carbon steel pipes with artificial wall-thinned flaws. Finally, a large strain FEA was conducted for the cases corresponding to non-planar flaws (θ was beyond the range in Netto et al. or Oh et al.'s work) to simulate and verify the experimental results.

2. Experiment

2.1 Burst test system

A diagram of the burst test system is shown in Fig. 2. All tests were conducted at room temperature. In the tests, an internal pressure p was applied by gradually injecting water into the pipe using a hydro pump.

The test specimen configuration is shown in Fig. 3. The dimensions of the artificial flaw and burst pressure p_f for each test specimen with a nominal outer diameter 107.1 mm (100A) are shown in Table 1. The burst pressure p_f was defined as the average pressure attained during the 2 seconds surrounding the observed maximum value, measured at intervals of 0.01 seconds. The specimen material was carbon steel of type JIS (Japanese Industrial Standards) STPT 370. The chemical compositions and tensile strengths of the specimens are shown in Table 2.

2.2 Experimental results

First, the effect of the circumferential angle of the non-planar flaw (θ in Fig. 1, left) on the burst pressure, which is not considered for an axial crack, was evaluated. To this end, the burst pressure p_f obtained from the current experiment was compared with p_1 in Figs. 4 and 5.

$$p_1 = \frac{2t_1}{\sqrt{3}R_\mathrm{i}}\sigma_\mathrm{f} \tag{1}$$

Here, R_i is the inner radius of the sound cylinder, t_1 is the flaw ligament thickness, and σ_f is the flow stress defined as an average of the nominal tensile stress σ_B0 and the nominal yield stress σ_y0. Equation (1) gives a burst pressure for the cylinders with a wall thickness of t_1, and p_1 is the internal pressure when the elastic-perfectly plastic material reaches the fully plastic state for a material with yield strength σ_f (Hill, R., 1950). The definitions of θ_eq and δ_zeq in Figs. 4 and 5 are as follows.

$$\theta_\mathrm{eq} = \left[\theta + \frac{1}{R_\mathrm{m}}\left\{(R_\mathrm{o} - t_1)\theta + \frac{2(t - t_1)}{\tan(10°)}\right\}\right] \Big/ 2 \tag{2}$$

$$\delta_{\mathrm{zeq}} = \delta_{\mathrm{z}} + \frac{(t - t_1)}{\tan(10°)} \tag{3}$$

Here, θ_{eq} was defined as the value at which the area of a rectangle with sides θ_{eq} and (t-t_1) is equivalent to the value of the actual area of the cross section of a flaw. δ_{zeq} in Eq. (3) is similar, as well.

Fig. 4 shows the case of p_{f}/p_1 with $t_1/t = 0.5$. This figure demonstrates that p_{f} is affected by θ_{eq}. The value of p_{f} decreased with an increase in θ_{eq} when δ_{z} was large enough ($\delta_{\mathrm{z}} \geq 100$ mm). For example, the decrease in p_{f} is approximately 40% for $\delta_{\mathrm{z}} \geq 100$ mm, and p_{f} was nearly identical to p_1 when $\theta_{\mathrm{eq}}/2\pi = 1$. Thus, p_{f}/p_1 is approximately 1 when δ_{z} and θ_{eq} are large. In contrast, when θ_{eq} and $\delta_{\mathrm{z}} \rightarrow 0$, it appears that $p_{\mathrm{f}}/p_1 \rightarrow t/t_1 = 2$. That is, it is predicted that the burst pressures are close to p_{f} in pipes of wall thickness t when θ_{eq} and $\delta_{\mathrm{z}} \rightarrow 0$, and they are equal to p_{f} in pipes of wall thickness t_1 when δ_{z} and θ are great. This effect of θ on p_{f} means that the strength decreases with an increase in θ, so the effect of θ on p_{f} should be taken into consideration. However, the effect of θ on p_{f} decreases with a decrease in δ_{z}, and this effect was small when $\delta_{\mathrm{z}} \leq 50$ mm.

Figure 5 shows p_{f}/p_1 for the cases where $t_1/t = 0.75$, 0.5, and 0.25 with $\delta_{\mathrm{z}} = 50$ mm. According to Fig. 5, the effect of θ on p_{f} is small (approximately 10%) in cases where $t_1/t = 0.75$ and 0.5 with $\delta_{\mathrm{z}} = 50$ mm. In contrast, the effect of θ on p_{f} is large (approximately 30%) for $t_1/t = 0.25$ when δ_{z} is 50 mm. Therefore, clearly both δ_{z} and t_1/t are correlated with a result of p_{f} decreasing as θ increases.

In summary, from the experimental results, θ tended to affect p_f for the cases with large δ_z, and t_1/t was also correlated with a decrease in p_f as θ increased.

3. Finite element analysis

The MARC finite element code was used for the large strain elastic-plastic FEA model. In this analysis, the pipes for the FEA model are chosen specifically to examine the effect of θ on p_f:

1） To validate the FEA results; the experimental results and the FEA results were compared (p^{FEA}/p_f of 9 analysis cases shown in Table 3).

2） To reproduce the effect of p_f decreasing with the increase of θ; values of p_f are compared for $\theta/2\pi = 1/12$ and 1 (p^{FEA}/p_1 of 10 analysis cases shown in Table 4).

3） To reproduce the effect of p_f decreasing with the increase of θ and affected by t_1/t; pipes with $\theta/2\pi = 1/12$, 1 and $\delta_z = 50$ mm in $t_1/t = 0.75, 0.5, 0.25$ are chosen (p^{FEA}/p_1 of 6 analysis cases shown in Table 5).

Note that $\theta/2\pi \geq 1/12$ was chosen to consider the effect of θ on p_f for cases of non-planar flaws.

Three-dimensional models of the pipes with the flaws shown in Tables 3 through 5 and in Fig. 3 were developed using the MARC software, including models with mesh refinement in the wall-thinned zone. In each case, one quarter of the specimen was modeled because of symmetry conditions, as shown in Fig. 6. All models used 20-node brick elements. The number of elements and nodes range from 17,660 elements/85,840 nodes to 23,650 elements/111,181 nodes. The material behavior was assumed to be governed by the J2-incremental theory of plasticity, the isotropic hardening rule and Prandtl-Ruess flow theory. The Newton-Raphson iterative method was used for nonlinear convergence. The Young's modulus E was equal to 206 GPa, and the Poisson's ratio ν was 0.3. The true stress σ_t -true strain (plastic) ε_t curve used in the large strain FEA is shown in Fig. 7. The values of σ_t and ε_t shown in Fig. 7 were evaluated under the assumption of constant volume, such that $\sigma_t = \sigma_n (1+\varepsilon_n)$ and $\varepsilon_t = \ln (1+\varepsilon_n)$, where σ_n is the nominal stress, and ε_n is the nominal strain obtained from a tensile test for heat ID b in Table 2.

The boundary conditions are shown in Fig. 6. The load (up to the internal pressure, at which the outer surface circumferential stress of the sound cylinder reached $0.2\sigma_{y0}$) was applied via an even incremental loading procedure of approximately 10 steps. After this loading, MARC's automatic load-stepping option was applied up to p^{FEA} under the restriction that the strain increment in a given load increment was less than 2% of the previous total strain. In addition, MARC's "follower force" option was specified to ensure that the geometric non-linear effects were included, and therefore, the internal pressure was always applied perpendicularly to the current (deformed) inner surface of the cylinder. The internal pressure p and thrust stress $\sigma_m = p\pi 49.55^2/\{\pi(56.15^2-49.55^2)\} = 3.52p$ MPa were also applied on the cylinder end. Here, the internal pressure at which the Von Mises stress exceeded the true tensile stress σ_B throughout the ligament thickness in the flaw center, shown in Fig.

6 (b) as “evaluated line,” was designated as p^{FEA}.

Figure 8 shows the typical Von Mises stress distribution at p^{FEA} for the cases with flaws $\delta_z = 50$ mm and $\theta/2\pi = 1/12$. In Fig. 8, the zones where the Von Mises stress exceed the true tensile stress $\sigma_B = 543$ MPa are colored gray. As shown in this figure, the pressure at which the gray zone penetrated the wall-thickness in the flaw center was defined as the predicted burst pressure p^{FEA}, and p^{FEA} values for all cases are summarized in Tables 3 through 5.

3.1 FEA results: Validation

According to the 9 analysis cases shown in Table 3, the discrepancies between p^{FEA} and p_f are small (approximately -8 % to +8 %). In Fig. 9, p^{FEA}/p_f is plotted for $t_1/t = 0.75$, 0.5, and 0.25 with $\theta/2\pi = 1$ (that is, the 9 cases in Table 3) to examine the relationship between the flaw configuration and calculation accuracy.

It can be observed from Fig. 9 that the value of p^{FEA} is non-conservative for $t_1/t = 0.75$ and 0.25, and conservative for $t_1/t = 0.5$. This means that the p_f prediction accuracy was similar for the same values of t_1/t, even though δ_z changed. Specifically, in the case of $t_1/t = 0.75$, p^{FEA}/p_f is approximately 1.08 (the range of δ_{zeq} is 80 to 160 mm). In the case of $t_1/t = 0.25$, p^{FEA}/p_f is approximately 1.00 (the range of δ_{zeq} is 130 to 180 mm). In the case of $t_1/t = 0.5$, p^{FEA}/p_f is 0.92 to 1.00 (the range of δ_{zeq} is 70 to 170 mm).

With regards to these discrepancies in p_f and p^FEA, one cause might be the difference in the flaw ligament thickness between the designed value (value in FEA) t_1 and the measured value $t_{1\mathrm{measured}}$. In the case of $t_1/t = 0.25$, where $p^\mathrm{FEA}/p_\mathrm{f}$ is approximately 1.00, $t_1/t_{1\mathrm{measured}}$ is smaller than 1 ($t_1/t_{1\mathrm{measured}}$ is approximately 0.95). In addition, in the case of $t_1/t = 0.5$, $p^\mathrm{FEA}/p_\mathrm{f}$ increased from 0.92 to 1.02, though $t_1/t_{1\mathrm{measured}}$ decreased from 1.01 to 0.95. Thus, the cause is not clear, which is an issue that should be resolved in future work. However, the discrepancy between p_f and p^FEA was approximately 10% overall, and it was concluded that the p_f prediction of the FEA model was satisfactory.

3.2 FEA results: The effect of θ on p^{FEA}

Next, from the results of the 10 analysis cases shown in Table 4, p^FEA values corresponding to the cases in Fig. 4 were plotted with solid marks in Fig. 10 by comparing the two p^FEAs for the cases of $\theta/2\pi = 1/12$ and 1. As observed in Fig. 10, the decrease in burst pressure with the increase in θ as predicted by FEA was approximately 8% for the case of $\delta_\mathrm{z} = 50$ mm and approximately 15% for $\delta_\mathrm{z} = 145$ mm. Similarly, when the decreased burst pressure p_f for $\theta/2\pi = 1/12$ and 1 was interpolated from the experimental results, the value was approximately 7% for $\delta_\mathrm{z} = 50$ mm and approximately 20% for $\delta_\mathrm{z} = 145$ mm. Thus, the effect of p_f decreasing as θ increased was confirmed not only by experiment (p_f), but also by the FEA (p^FEA) model.

3.3 FEA results: The effect of t_1/t for p^{FEA}

Finally, an attempt was made to reproduce the observation that a decrease in p_f with an increase of θ is affected by t_1/t. As mentioned above, according to Fig. 5, the effect of θ on p_f is small (approximately 10%) when $t_1/t = 0.75$ and 0.5 and δ_z is 50 mm. However, the effect of θ on p_f is considerable (approximately 30%) when $t_1/t = 0.25$ and δ_z is 50 mm.

The elastic-plastic FEA simulations were performed for this purpose, as shown in Table 5. p^FEA and p_1 were compared in the normalized form in Fig. 11. Figure 11 shows the cases for p_f/p_1 with and p^FEA/p_1 for $\delta_\mathrm{z} = 50$ mm, with $t_1/t = 0.75$, 0.5, and 0.25. In Fig. 11, open and closed marks represent the cases of p_f/p_1 and p^FEA/p_1, respectively.

In the cases of $t_1/t = 0.75$ when δ_z is 50 mm, the effect of θ on p^FEA is small (approximately 5%) for the range of $\theta/2\pi = 1/12$ to 1. In contrast, in the cases of $t_1/t = 0.25$ when δ_z is 50 mm, the effect of θ on p^FEA in the same range of θ is large (approximately 20 %). Similarly, when the decrease in burst pressure p_f for $\theta/2\pi = 1/12$ and 1 was interpolated from the experimental results, the value was approximately 7% for $t_1/t = 0.50$ and approximately 27% for $t_1/t = 0.25$. Therefore, it is clear that t_1/t correlated with a decrease in burst pressure as θ increases, which was confirmed not only by experiment (p_f) but also by FEA (p^FEA) in Fig. 11.

In summary, from the large strain elastic-plastic FEA results, trends in the experimental results (that is, θ tended to affect p_f for the cases with larger δ_z, and t_1/t was also correlated with a decrease in p_{f} with the increase of θ) were successfully simulated.

3.4 FEA results: The relationship between internal pressure and radial displacement

A theoretical equation for radial displacement at radius r in the elastic region ($c < r \leq R_0$) of an elastic-perfectly plastic sound cylinder under internal pressure is known to be as follows (Allan F. B., 2009):

$$u_r = \frac{(1+\nu)\cdot c^2 \cdot R_{\mathrm{o}}^2 \cdot p_c}{E\cdot\left(R_{\mathrm{o}}^2 - c^2\right)}\cdot\left\{\frac{1}{r} + (1 - 2\cdot\nu)\cdot\frac{r}{R_{\mathrm{o}}^2}\right\} \tag{4}$$

Here, c is the position of the elastic-plastic boundary and p_{c} was defined as follows:

$$p_c = p - \left(2\sigma_{\mathrm{y0}} / \sqrt{3}\right)\log\left(c / R_{\mathrm{i}}\right) \tag{5}$$

Considering that the burst pressure of the elastic-perfectly plastic cylinder p_{cf} is defined as p for $c \rightarrow R_{\mathrm{o}}$, i.e., $u_{\mathrm{r}}|_{r = R\mathrm{o}} \rightarrow \infty$, u_{r} at the outer surface of the flaw center, u_{ro} was focused as follows.

For reference, two sound cylinders with R_{o} = 53.55 mm, an axial length of 170 mm and thicknesses of 2 and 4 mm were analyzed. The deformation of the two sound cylinders and wall-thinned pipes with t_1/t = 0.5 up to p^{FEA} are compared in Fig. 12. As designated in Fig. 12, u_{ro}

was plotted for p in Fig. 13. Here, the maximum p of wall-thinned pipes was p^{FEA}.

Interestingly, in spite of partial wall-thinning, a characteristic of $u_{\mathrm{ro}} \rightarrow \infty$ was confirmed in Fig. 13 for the value near p^{FEA}. For the FEA results of $\theta/2\pi = 1$, these results were similar to the results for a sound cylinder with t = 2 mm (that is t_1 in wall-thinned pipes). In contrast, regarding FEA results of $\theta/2\pi = 1/12$ (that is $\theta \rightarrow 0$), these results seemed to approach a result in a sound cylinder with t = 4 mm (that is t in wall-thinned pipes). The above seemed to show the mechanism for how θ affected p_{f}. In addition, regarding the FEA results for $\theta/2\pi = 1$, the effect of δ_{z} on internal pressure in $u_{\mathrm{ro}} \rightarrow \infty$ was large, and these results were similar to the result of a sound cylinder with t = 2 mm (that is, t_1 in wall-thinned pipes) when δ_{z} was large. In contrast, regarding the FEA results of $\theta/2\pi = 1/12$ (that is, $\theta \rightarrow 0$), the effect of δ_{z} on internal pressure in $u_{\mathrm{ro}} \rightarrow \infty$ was small compared to when $\theta/2\pi = 1$. The above analysis showed the effect of θ on decreasing p_{f} with a decrease in δ_{z}. From the above observations, it seems reasonable to estimate the upper bound of the effect of θ on p_{f} as $(t/t_1 - 1)$.

4. Discussion

It may be more effective to define p^{FEA} as the pressure when accumulated strain first reaches failure strain, such as the approach shown by Oh et al. (2006). However, as Oh et al. themselves admit, “the failure criterion based on failure strain suggests that failure is governed by global plastic instability, and thus these experimental data in a corrosion defect (that is non-planar flaw) are not appropriate to validate the present approach". The FEA model in this paper was a pipe with a modified non-planar flaw, and the maximum Von Mises strain in p^{FEA} was approximately 20%, which was considerably smaller than the failure strain. Therefore, the failure criterion based on the failure strain was thought to be inappropriate to apply to the case considered in this paper. Another piece of evidence suggesting that this might be inappropriate was that collapse occurred before burst, as demonstrated in Fig. 13. In addition, p^{FEA} obtained by the σ_{B}-based failure criterion, was very close to the pressure from $u_{\mathrm{ro}} \rightarrow \infty$. Considering that the p^{FEA} obtained for a case p_{f} of tested specimens was close to the experimental result p_{f}, and p^{FEA} seemed to simulate the pressure corresponding to collapse, it seems that using p^{FEA} is acceptable for cases without experimental results.

5. Conclusion

In this paper, the effect of the circumferential angle θ on the burst pressure p_{f} was confirmed experimentally using the burst test and numerically via a large strain elastic-plastic FEA simulation. From the experimental results, θ tended to affect p_{f} for cases with large δ_{z}, and additionally, t_1/t was correlated with a decrease in p_{f} accompanied by an increase of θ. These tendencies were successfully simulated by the elastic-plastic FEA model. The effect was as large as 30 % in the case of $t_1/t = 0.25$ and 40 % in the case of $\delta_{\mathrm{z}} = 145$. The mechanism how θ affected p_{f} was explained as the upper bound FEA pressure (at which collapse is observed) for a flaw with small θ was close to that of a sound cylinder with thickness t, and the value for large θ was close to that of a sound cylinder with t_1. From the above observations, it seems reasonable to estimate the upper bound of the effect of θ on p_f as (t/t_1 - 1). This effect means that the burst pressure predicted for a crack with identical ligament thickness decreases with an increase in θ, such that the effect of θ on p_f should be taken into consideration in evaluating p_f.

Nomenclature

a: depth of a constant-depth axial crack

p: internal pressure

p_1: internal burst pressure predicted for a sound cylinder with thickness t_1; Eq. (1)

p^{FEA}: internal burst pressure predicted by FEA

p_{f}: internal burst pressure

t: wall thickness of a pipe

t_1: flaw ligament thickness

$t_{1\mathrm{Measured}}$: flaw ligament thickness; measured

u_{r}: radial displacement; Eq. (4)

u_{ro}: u_{r} at the outer surface of the flaw center

D_{o}: outer diameter of a pipe

E: Young's modulus

R_{i}: inner radius of a pipe

R_{m}: mean radius of a pipe

R_{o}: outer radius of a pipe

δ_{z}: axial length of a planar or a non-planar flaw

δ_{zeq}: equivalent δ_{z}; Eq. (2)

ε_{F0}: elongation

ε_n, ε_t: nominal and true strain

ν: Poisson's ratio

θ: circumferential angle of a non-planar flaw

θ_{eq}: equivalent θ; Eq. (3)

σ_B: true tensile stress

σ_{B0}: nominal tensile stress

σ_f: flow stress

σ_n, σ_t: nominal and true stress

σ_m: thrust stress

σ_{y0}: nominal yield stress

List of Tables

Table 1 Dimensions of the artificial flaws and experimental data

Table 2 Chemical composition and tensile strength of the specimens (JIS STPT 370)

Table 3 FEA results: Validation

Table 4 FEA results: The effect of θ on p^{FEA}

Table 5 FEA results: The effect of t_1/t for p^{FEA}

Table 1 Dimensions of the artificial flaws and experimental data

$\theta/2\pi$	$\theta_{eq}/2\pi$	t_1/t	$t_{1\mathrm{Measured}}$ (mm)	δ_z (mm)	δ_{zeq} (mm)	p_f (MPa)	p_f/p_1	Fracture mode	Ser.#	Heat ID. in Table. 2
1	1	0.75	2.97	145	156.34	26.58	1.00	axial	07-01	b
1	1	0.75	2.99	100	111.34	27.62	1.03	axial	07-02	b
1	1	0.75	2.96	95	106.34	27.76	1.05	axial	07-03	b
1	1	0.75	2.95	85	96.34	27.88	1.06	axial	07-04	b
1	1	0.75	2.90	75	86.34	28.17	1.09	axial	07-05	b
1	1	0.75	2.96	50	61.34	30.25	1.14	axial	07-06	b
1	1	0.50	2.00	145	167.69	16.50	0.94	axial	06-01	a
1	1	0.50	2.01	145	167.69	16.48	0.94	axial	06-02	a
1	1	0.50	1.94	145	167.69	16.44	0.97	axial	06-03	a
1	1	0.50	2.02	145	167.69	18.42	1.02	axial	07-07	b
1	1	0.50	2.03	145	167.69	19.00	1.05	axial	07-08	b
1	1	0.50	2.02	145	167.69	20.23	1.12	axial	07-09	b
1	1	0.50	1.99	100	122.69	18.35	1.05	axial	06-04	a
1	1	0.50	2.03	100	122.69	21.04	1.16	axial	07-10	b
1	1	0.50	1.99	80	102.69	21.01	1.18	axial	07-11	b
1	1	0.50	2.07	70	92.69	22.99	1.24	axial	07-12	b
1	1	0.50	1.98	60	82.69	22.69	1.28	axial	07-13	b
1	1	0.50	1.96	50	72.69	22.33	1.30	circ.	06-05	a
1	1	0.50	2.00	50	72.69	22.17	1.27	circ.	06-06	a
1	1	0.50	1.98	50	72.69	26.51	1.50	circ.	07-14	b
1	1	0.50	1.95	6	6	40.42	2.17	Guillotine	08-04	d
1	1	0.50	-	1	1	40.08	2.10	Guillotine	08-02	d
1	1	0.25	1.05	145	179.03	9.39	1.00	axial	07-15	b
1	1	0.25	1.06	100	134.03	10.49	1.11	axial	07-16	b
1	1	0.25	1.02	60	94.03	13.32	1.46	circ.	07-17	b
1	1	0.25	1.04	50	84.03	14.12	1.52	circ.	07-18	b
1	1	0.25	0.95	40	74.03	14.43	1.70	circ.	07-19	b
2/3	0.737	0.50	2.44	145	167.69	22.62	1.03	axial	07-34	c
2/3	0.737	0.50	2.20	100	122.69	21.78	1.11	axial	07-35	b
2/3	0.737	0.50	2.12	50	72.69	26.39	1.39	axial	07-36	b
1/3	0.403	0.50	2.30	145	167.69	22.85	1.10	axial	07-31	c
1/3	0.403	0.50	2.21	100	122.69	23.60	1.19	axial	07-32	b
1/3	0.403	0.50	2.12	50	72.69	27.01	1.33	axial	07-33	d
1/6	0.237	0.50	2.24	100	122.69	23.17	1.08	axial	07-26	d
1/6	0.237	0.50	2.05	50	72.69	26.25	1.34	axial	07-27	d
1/6	0.237	0.50	2.17	6	6	40.46	1.95	axial	08-03	d
1/6	0.237	0.50	-	1	1	38.82	2.03	circ.	08-01	d
0.019	0.019	0.50	2.04	145	167.69	25.53	1.31	axial	08-10	d
0.019	0.019	0.50	2.03	100	122.69	26.07	1.34	axial	08-08	d
0.003	0.003	0.50	-	145	167.69	25.41	1.33	axial	08-09	d
0.003	0.003	0.50	-	100	122.69	25.76	1.35	axial	08-07	d
0.003	0.003	0.50	-	50	72.69	26.90	1.41	axial	08-05	d
0.003	0.003	0.75	2.99	50	61.34	35.24	1.23	axial	08-12	d
0.003	0.003	0.25	0.98	50	84.03	18.70	2.00	axial	08-11	d
0	0	1	3.96	0	0	34.44	0.97	axial	07-25	b

Table 2 Chemical composition and tensile strength of the specimens (JIS STPT 370)

Heat ID.	C	Si	Mn	P	S	σ_{y0} (MPa)	σ_{B0} (MPa)	σ_f (MPa)	ε_{F0}
Specified	< 0.25	0.10–0.35	0.30–0.90	< 0.035	< 0.035	> 215	> 370	–	> 0.30
a	0.15	0.19	0.48	0.017	0.008	311	441	376	0.38
b	0.17	0.20	0.67	0.017	0.007	316	452	383.5	0.34
c	0.20	0.22	0.55	0.023	0.010	310	465	387.5	0.42
d	0.22	0.19	0.69	0.015	0.002	333	487	410	0.38

Table 3 FEA results: Validation

$\theta/2\pi$	t_1/t	$t_{1\mathrm{Measured}}$ (mm)	$t_1/t_{1\mathrm{Measured}}$	δ_z (mm)	δ_{zeq} (mm)	p_f (MPa)	p^{FEA} (MPa)	p^{FEA}/p_f	Ser.#
1	0.75	2.97	1.01	145	156.3	26.58	28.56	1.07	07-01
1	0.75	2.99	1.00	100	111.3	27.62	29.67	1.07	07-02
1	0.75	2.96	1.01	50	61.3	30.25	32.34	1.07	07-06
1	0.50	2.03	0.99	145	167.7	19.00	19.09	1.00	07-07
1	0.50	2.03	0.99	100	122.7	21.04	20.44	0.97	07-10
1	0.50	1.98	1.01	50	72.7	26.51	24.48	0.92	07-14
1	0.25	1.05	0.95	145	179.0	9.39	9.57	1.02	07-15
1	0.25	1.06	0.94	100	134.0	10.49	10.45	1.00	07-16
1	0.25	1.04	0.96	50	84.0	14.12	13.77	0.98	07-18

Table 4 FEA results: The effect of θ on p^{FEA}

$\theta/2\pi$	$\theta_{eq}/2\pi$	t_1/t	δ_z (mm)	δ_{zeq} (mm)	p^{FEA} (MPa)	p^{FEA}/p_1	Heat ID. in Table. 2
1	1	0.50	145	167.7	19.09	1.07	b
4/6	0.70	0.50	145	167.7	19.84	1.11	b
3/6	0.54	0.50	145	167.7	20.30	1.14	b
2/6	0.37	0.50	145	167.7	20.80	1.16	b
1/6	0.20	0.50	145	167.7	21.59	1.21	b
1/12	0.12	0.50	145	167.7	21.76	1.22	b
1	1	0.50	100	122.7	20.44	1.14	b
1/12	0.12	0.50	100	122.7	22.97	1.29	b
1	1	0.50	50	72.7	24.43	1.37	b
1/12	0.12	0.50	50	72.7	26.57	1.49	b

Table 5 FEA results: The effect of t_1/t for p^{FEA}

$\theta/2\pi$	$\theta_{eq}/2\pi$	t_1/t	δ_z (mm)	δ_{zeq} (mm)	p^{FEA} (MPa)	p^{FEA}/p_1	Heat ID. in Table. 2
1	1	0.75	50	61.3	32.34	1.15	b
1/12	0.10	0.75	50	61.3	34.02	1.21	b
1	1	0.50	50	72.7	24.43	1.37	b
1/12	0.12	0.50	50	72.7	26.57	1.49	b
1	1	0.25	50	84.0	13.77	1.46	b
1/12	0.14	0.25	50	84.0	16.29	1.73	b

List of Figures

Fig. 1 Axial planar flaw and non-planar flaws (axially and circumferentially in length) in a cylinder

Fig. 2 Wall-thinned pipe burst test system diagram

Fig. 3 Test specimen configuration (Unit: mm)

Fig. 4 Effect of flaw configuration on burst pressure (t_1/t = 0.5)

Fig. 5 Effect of flaw configuration on burst pressure (δ_z = 50 mm)

Fig. 6 Wall-thinned straight pipe specimen and boundary condition

Fig. 7 True stress–true strain curve

Fig. 8 Von Mises stress distribution (case with flaw of δ_z = 50 mm, $\theta/2\pi$ = 1/12)

Fig. 9 Validation of FEA results ($\theta/2\pi$ = 1)

Fig. 10 Effect of θ on p_f by FEA (t_1/t = 0.5)

Fig. 11 Effect of t_1/t for p^{FEA}

Fig. 12 Deformed pipes at p^{FEA}

Fig. 13 Radial deformation at the outer surface of the flaw center

References

Allan F. B., 2009. Applied Mechanics of Solids. http://solidmechanics.org/

ANI/ASME B31.G., 1991. Manual for Determining the Remaining Strength of Corroded Pipelines.

Duan, X., Kozluk, M.J., Li, M., 2009. Low probability of in-service feeder rupture. ASME, Pressure Vessels and Piping Division Conference, PVP2009-77060.

Hasegawa, K., Meshii, T., Scarth, D. A., 2011. Assessment of piping field failures and burst tests on carbon steel pipes with local wall thinning using ASME section XI code case N-597-2. Transactions of ASME, Journal of Pressure Vessel Technology 133, 031101-1-10

Hill, R., 1950. The Mathematical Theory of Plasticity. Oxford.

Kiefner, J. F., Maxey, W. A., Eiber, R. J., Duffy, A. R., 1973. Failure Stress Levels of Flaws in Pressurized Cylinders. Progress in Flaw Growth and Fracture Toughness Testing, American Society for Testing and Materials, Philadelphia STP 536, 461-481.

Netto, T.A., Ferraz, U.S., Estefen, S.F., 2005. The effect of corrosion defects on the burst pressure of pipelines. J. Construct. Steel Res, 61, 1185-1204.

Oh, C.K., Kim, Y.J., Beak, J.H., Kim, Y.P., Kim, W.S., 2006. Ductile failure analyses for API X65 pipes based on local failure criteria. ASME, Pressure Vessels and Piping Division Conference, PVP2006-ICPVT-11- 93769.

Figure

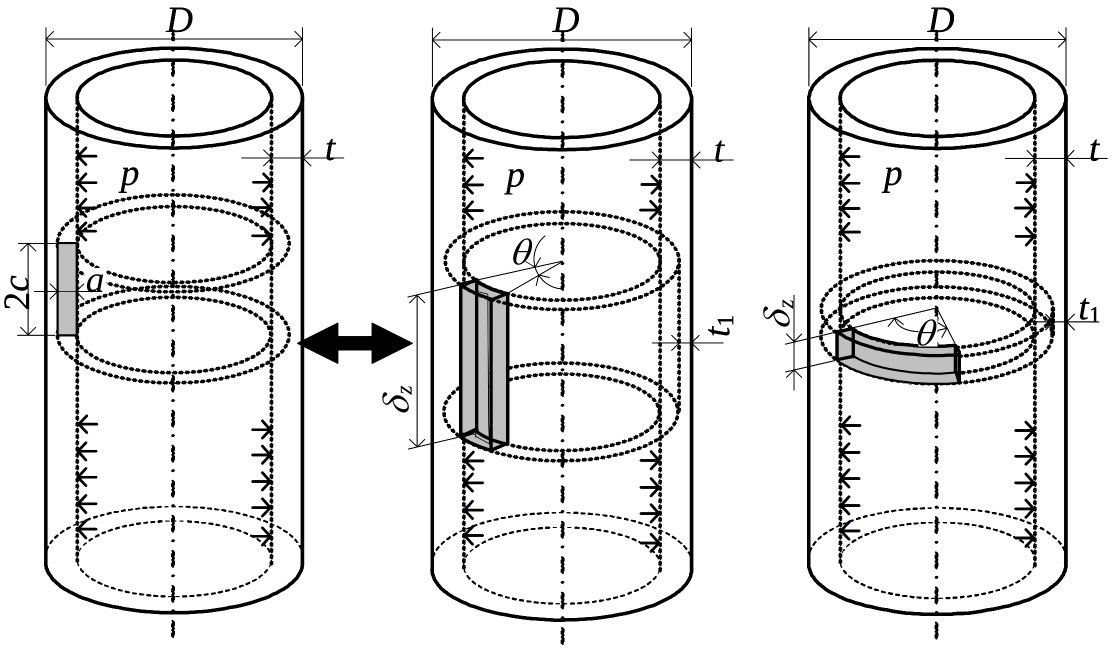

axial crack

wall thinning
(axially long)

wall thinning
(circ. long)

	crack	wall thinning
flaw depth	a	t-t_1
axial length	2c	δ_z
circ. length		θ

Fig. 1 Axial planar flaw and non-planar flaws
(axially and circumferentially in length) in a cylinder

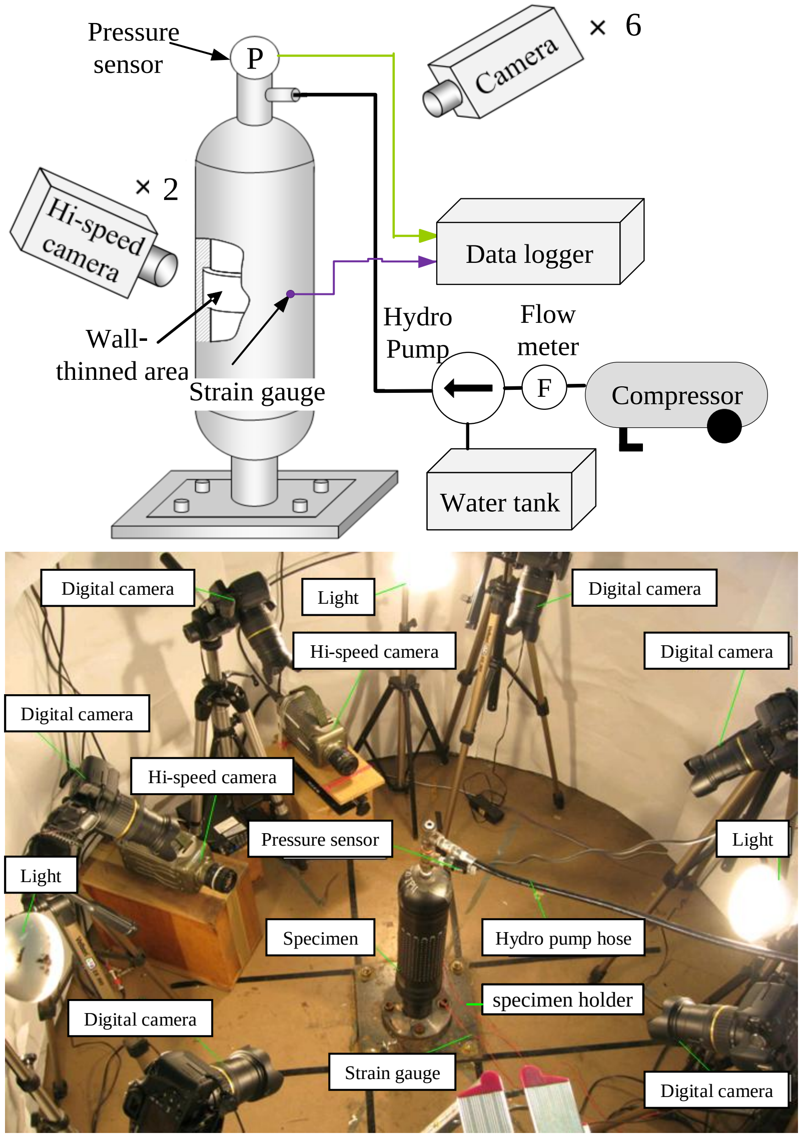

Fig. 2 Wall-thinned pipe burst test system diagram

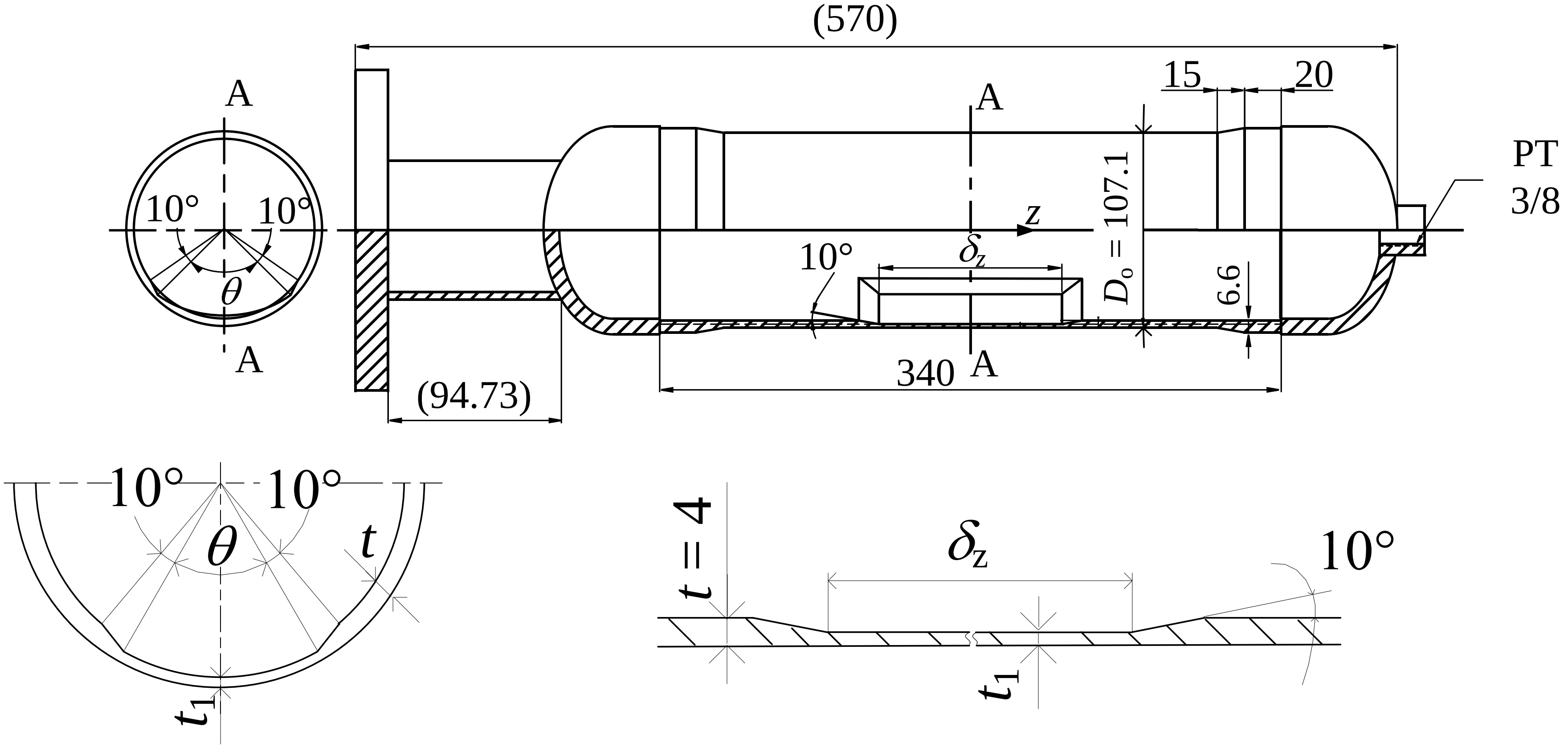

Fig. 3 Test specimen configuration (Unit: mm)

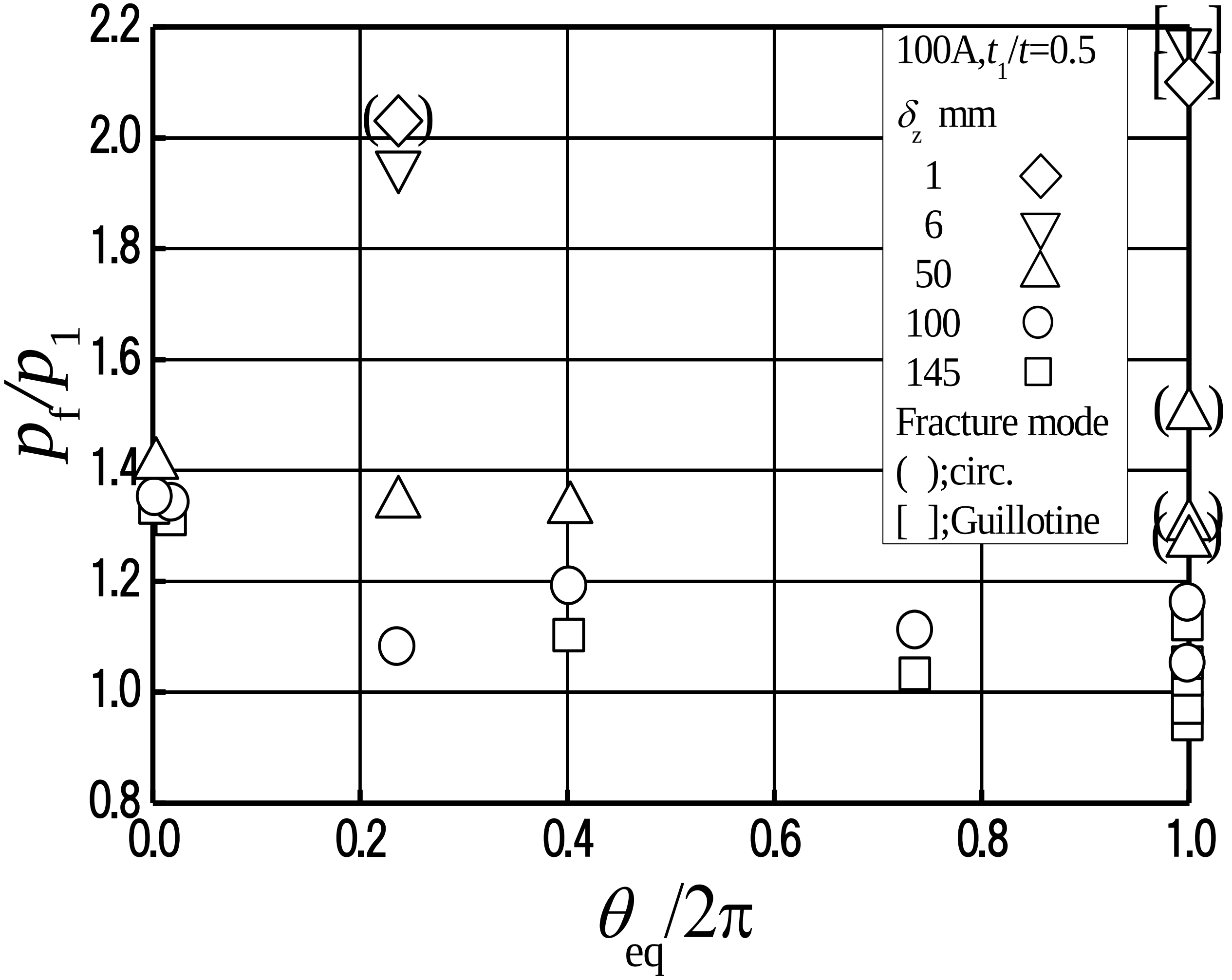

Fig. 4 Effect of flaw configuration on burst pressure ($t_1/t = 0.5$)

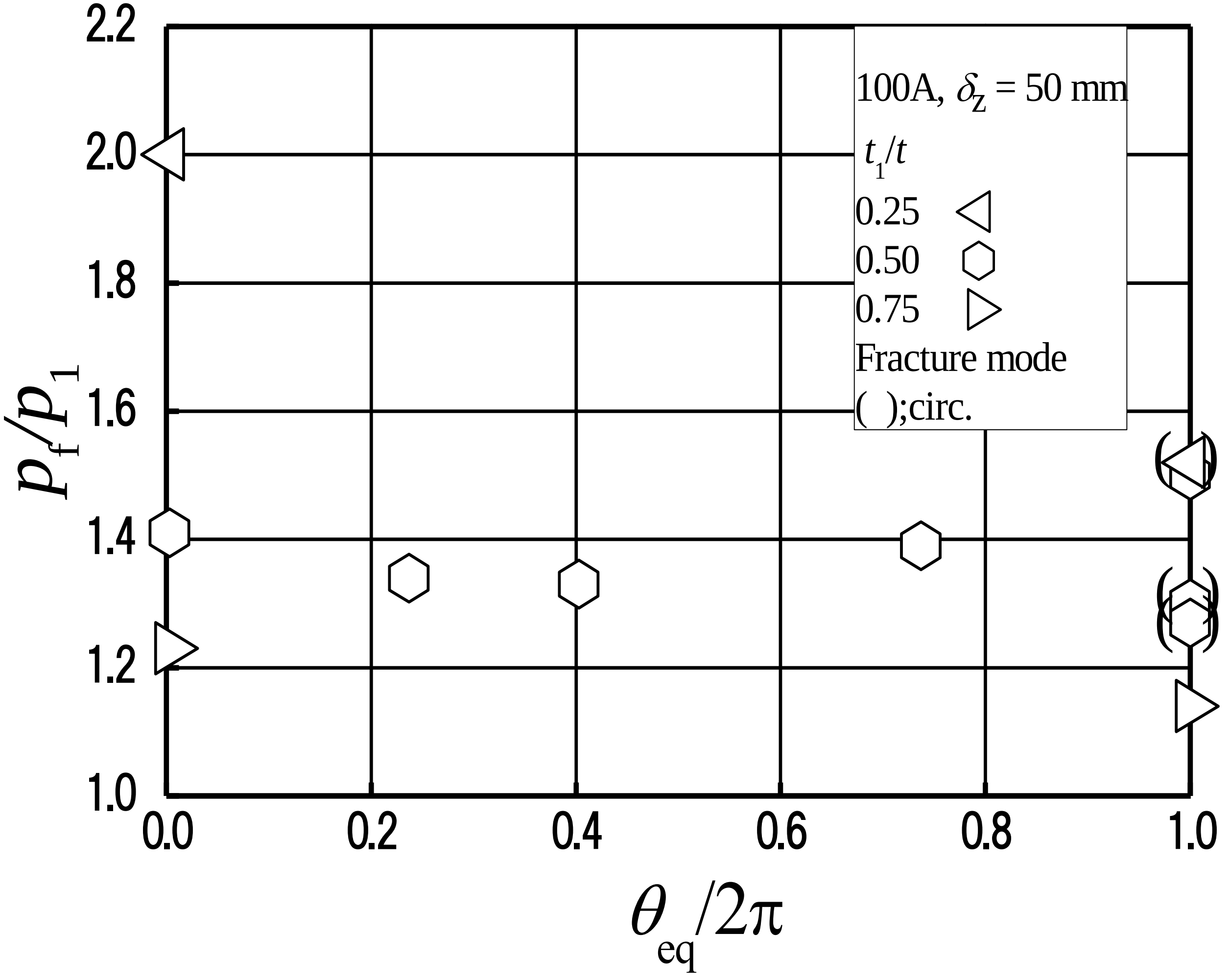

Fig. 5 Effect of flaw configuration on burst pressure (δ_z = 50 mm)

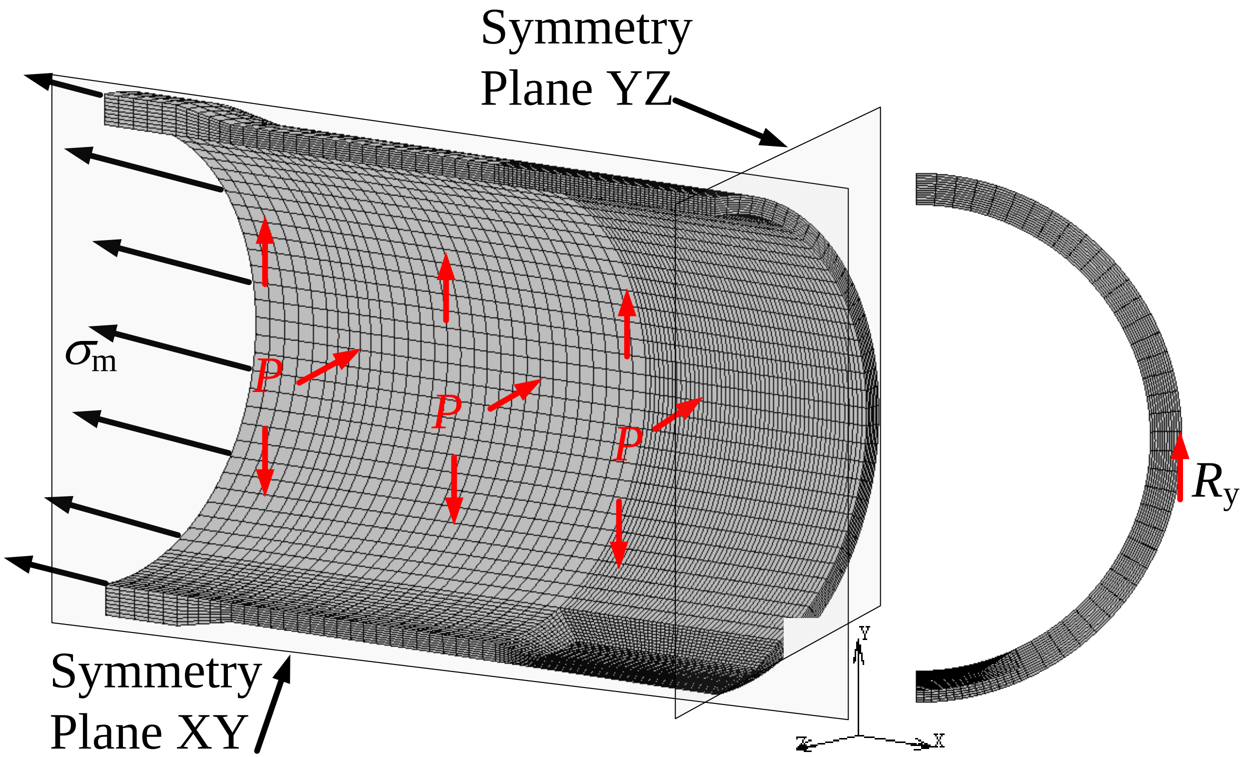

(a) FEA model and boundary conditions

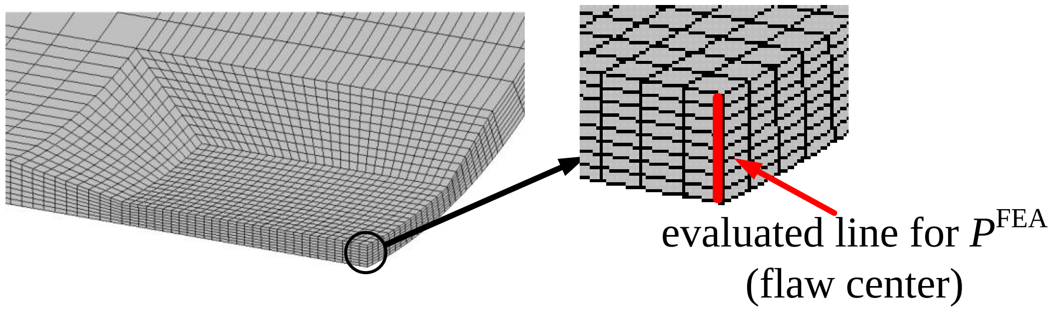

(b) Flaw area

Fig. 6 Wall-thinned straight pipe specimen and boundary condition

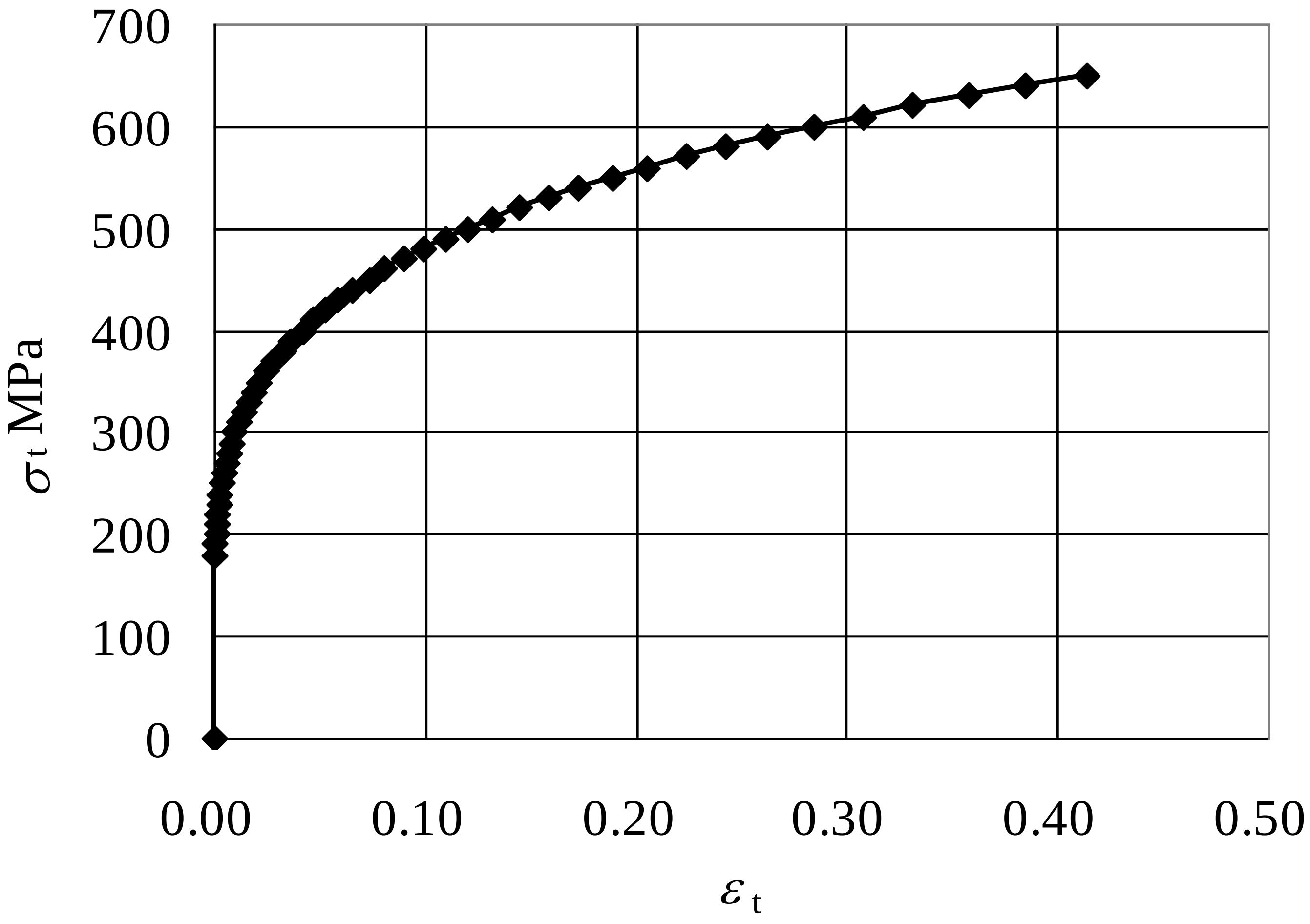

Fig. 7 True stress–true strain curve

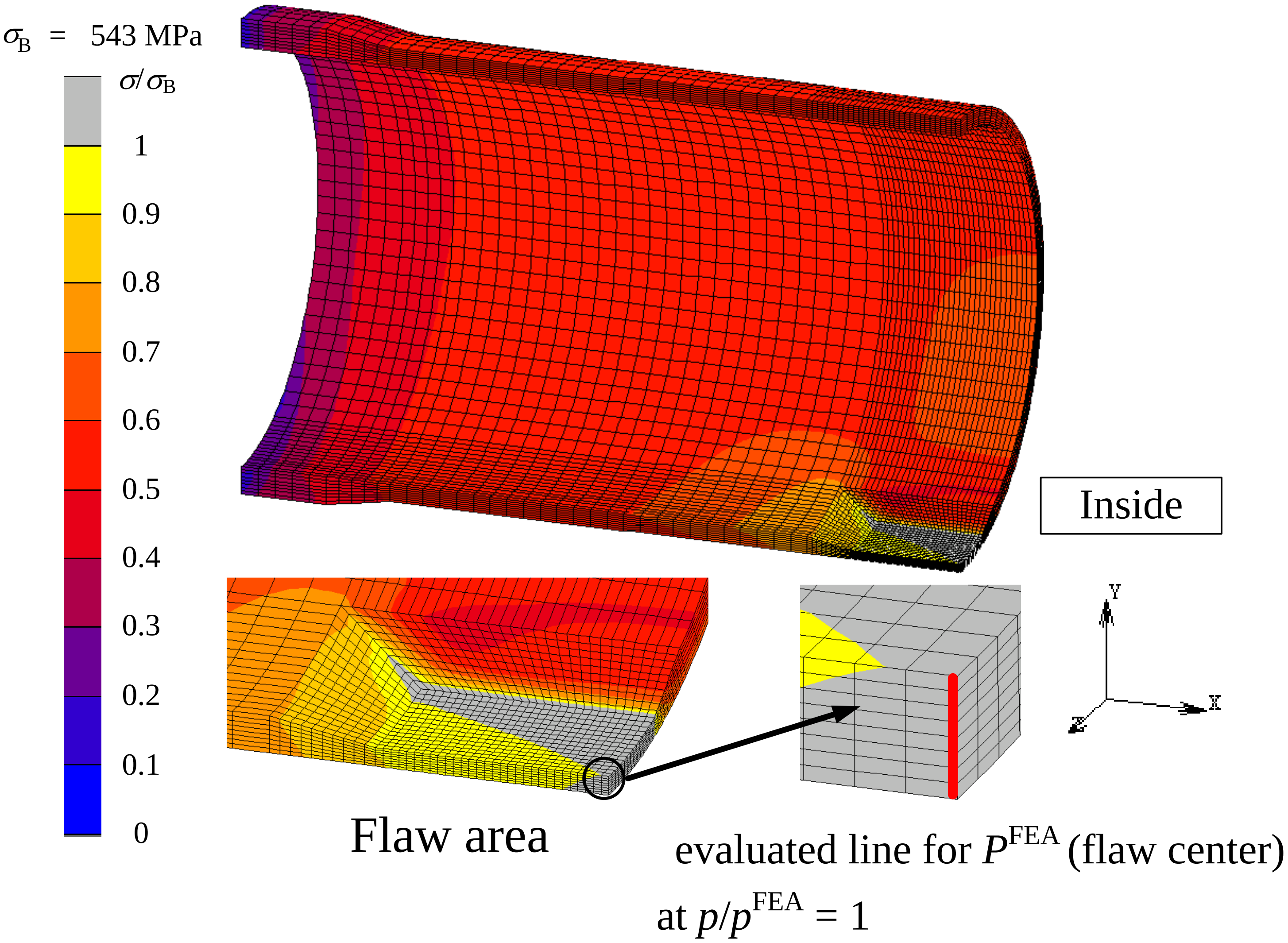

Fig. 8 Von Mises stress distribution (case with flaw of δ_z = 50 mm, $\theta/2\pi = 1/12$)

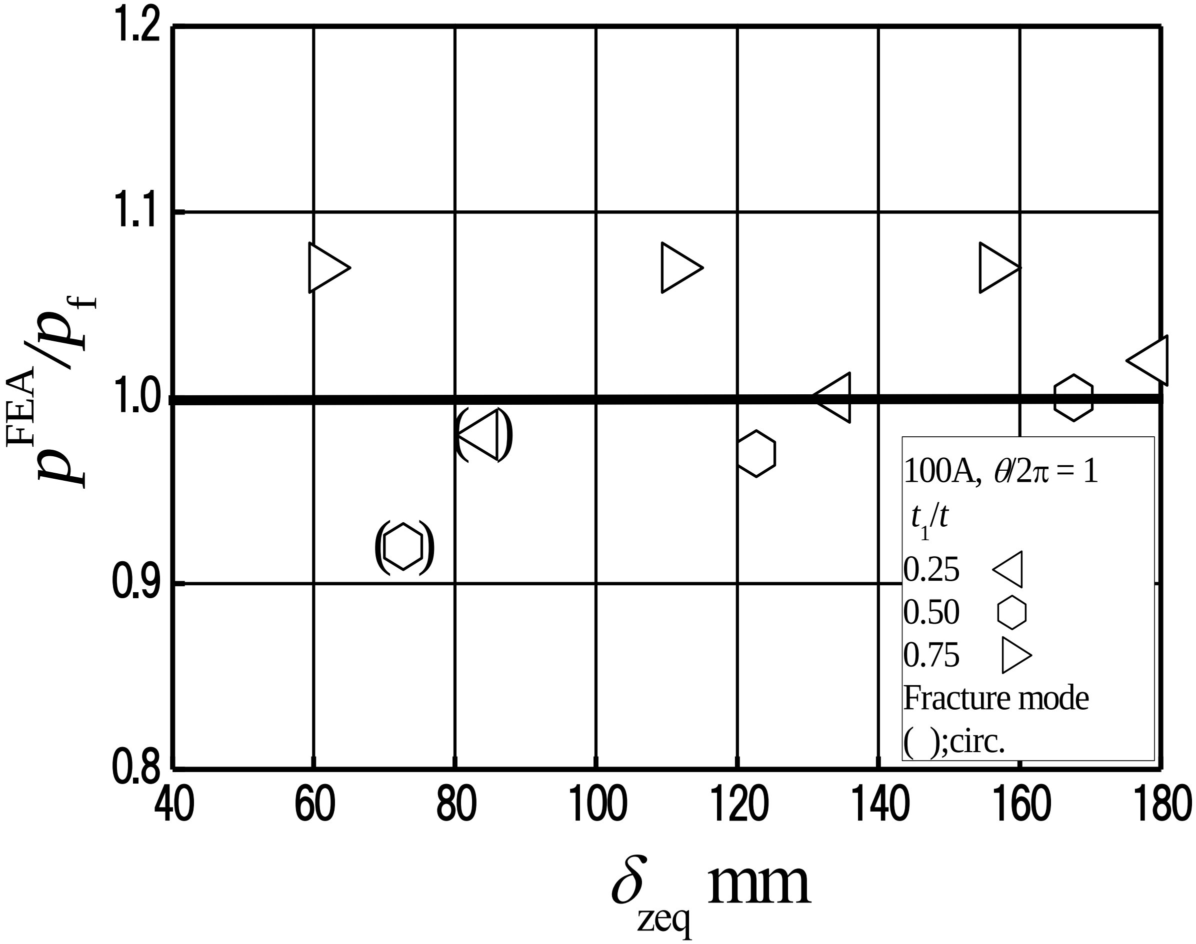

Fig. 9 Validation of FEA results ($\theta/2\pi = 1$)

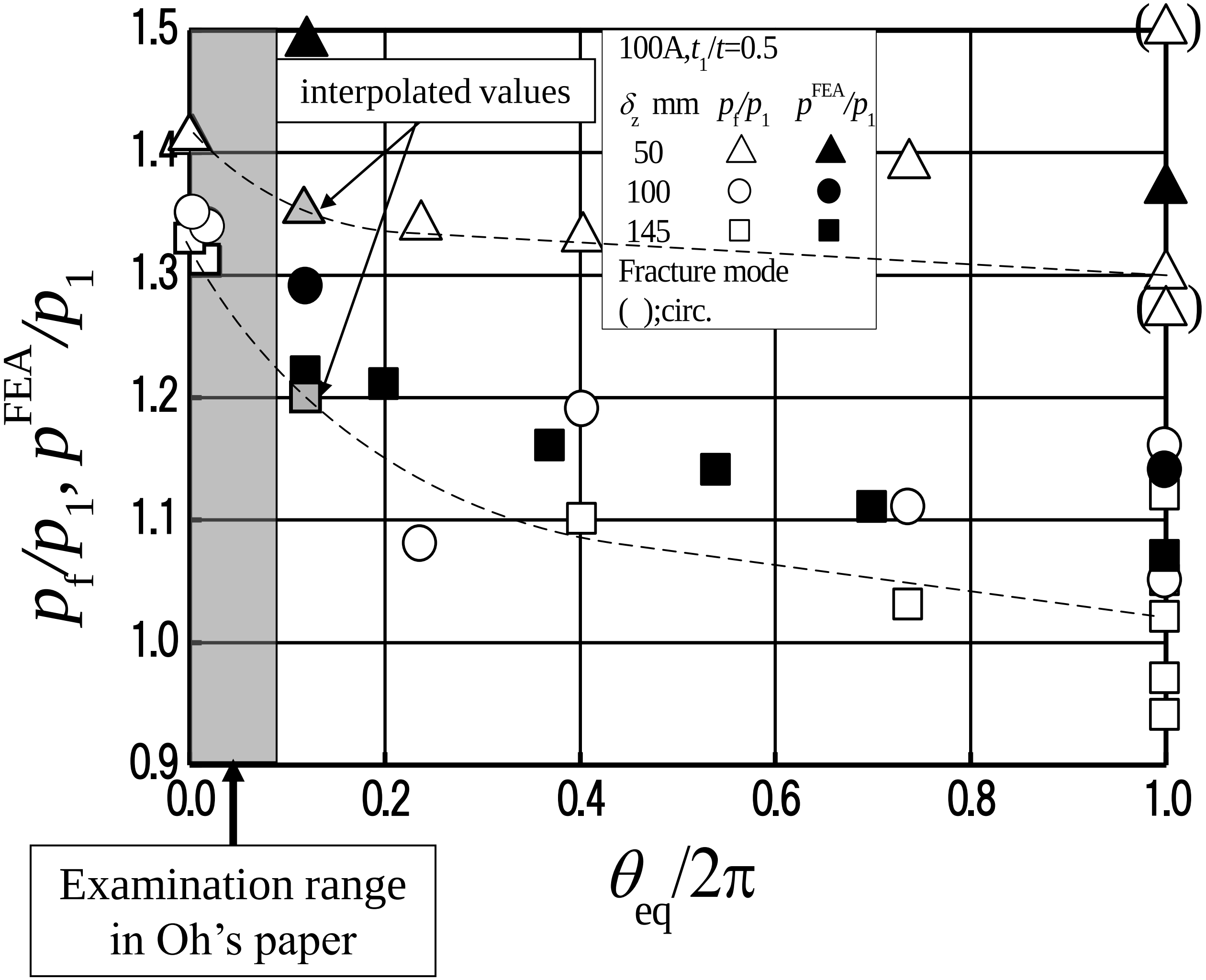

Fig. 10 Effect of θ on p_f by FEA ($t_1/t = 0.5$)

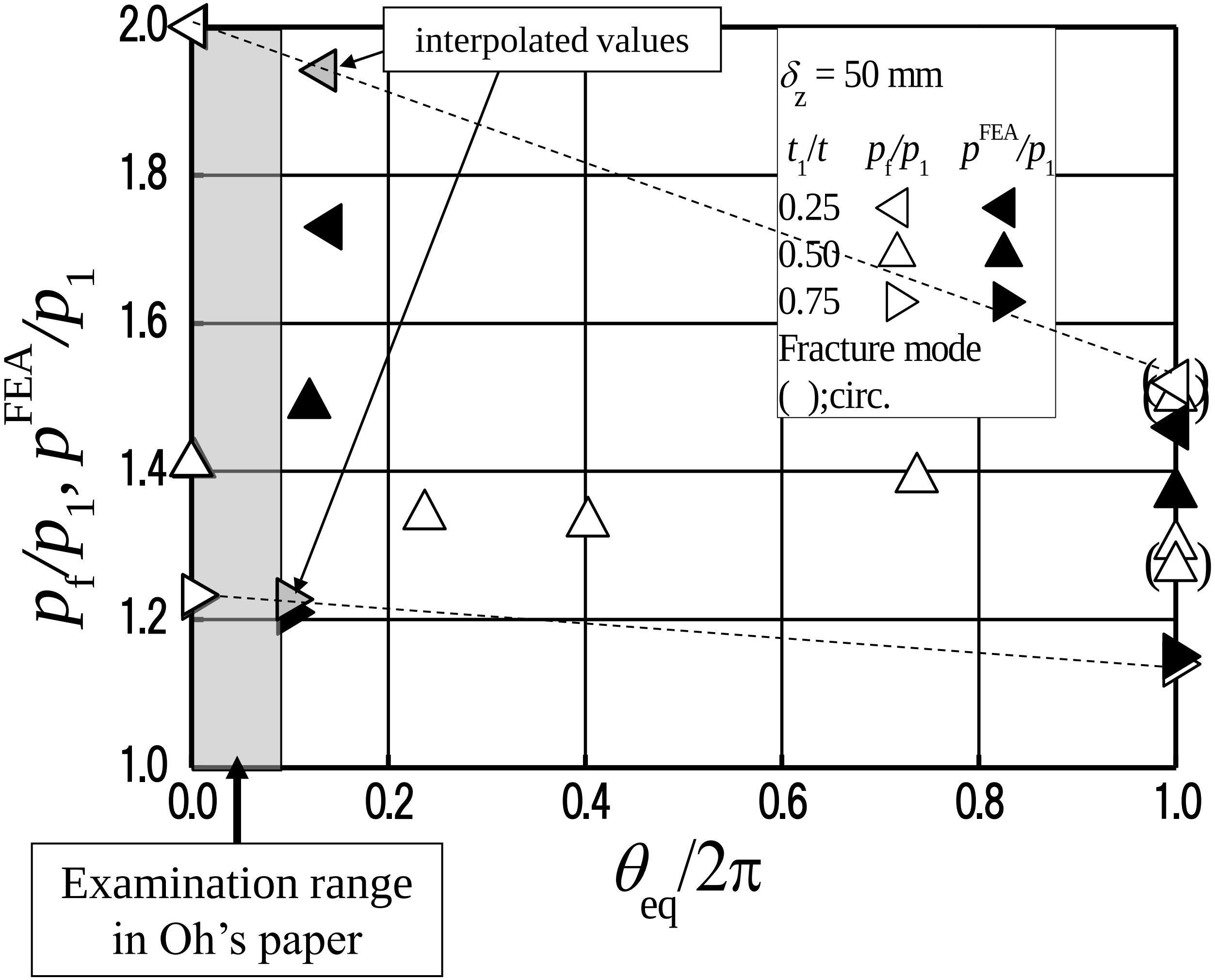

Fig. 11 Effect of t_1/t for p^{FEA}

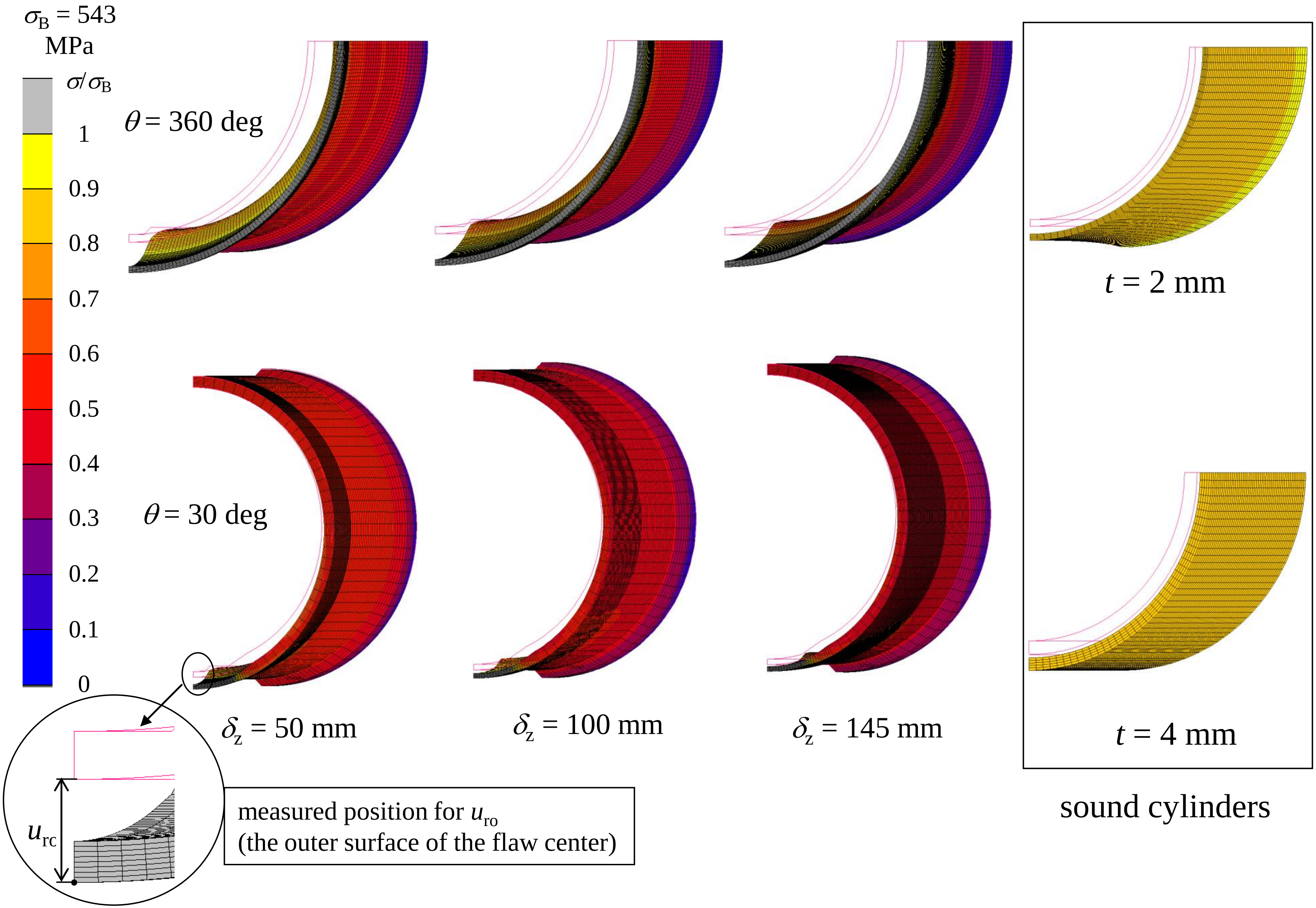

Fig. 12 Deformed pipes at p^{FEA}

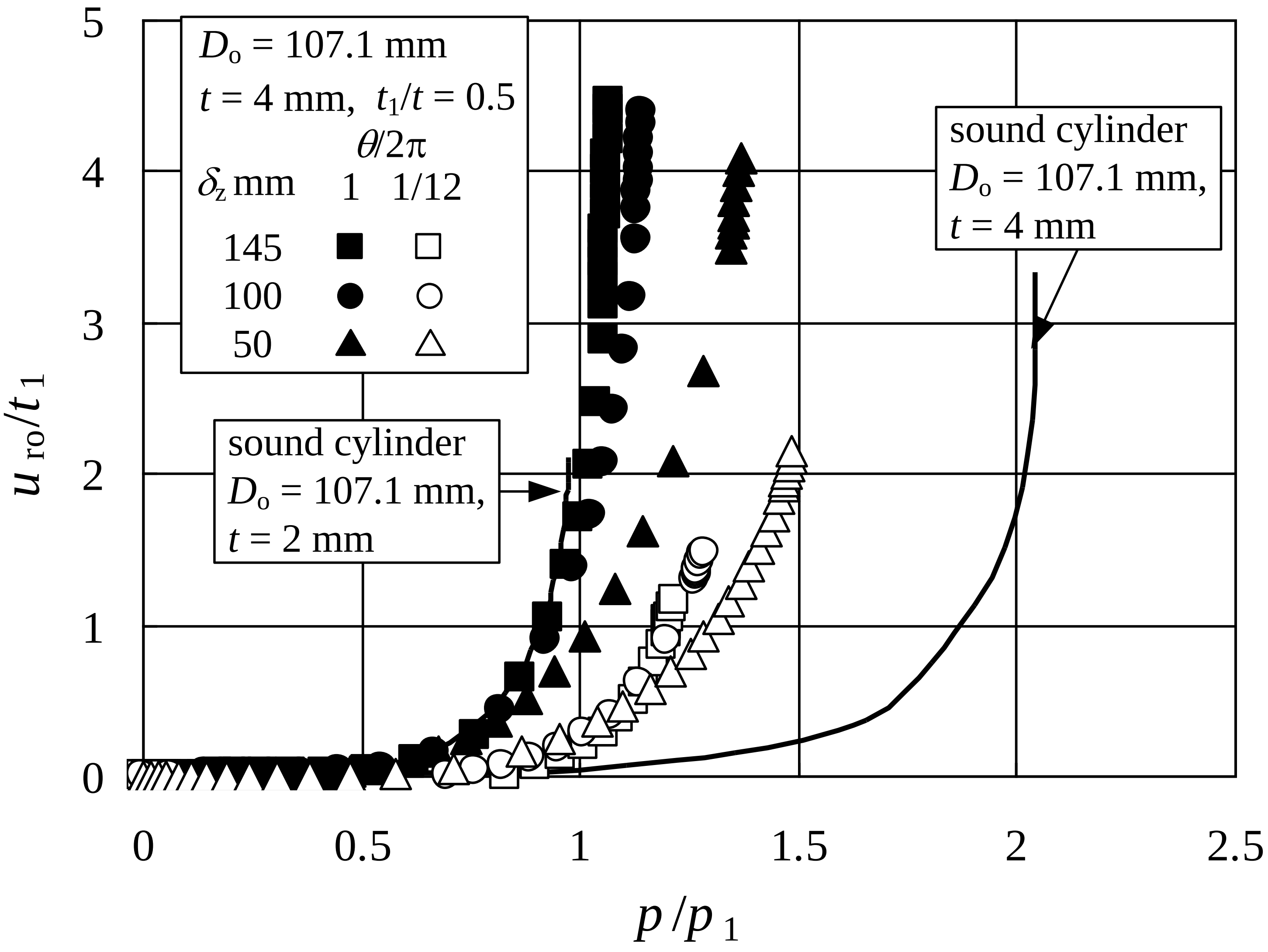

Fig. 13 Radial deformation at the outer surface of the flaw center